ACS APPLIED MATERIALS & INTERFACES

www.acsami.org

Research Article

High-Density Patterning of InGaZnO by CH_4: a Comparative Study of RIE and Pulsed Plasma ALE

Shreya Kundu,* Stefan Decoster, Philippe Bezard, Ankit Nalin Mehta, Harold Dekkers, and Frederic Lazzarino

Cite This: https://doi.org/10.1021/acsami.2c07514

Read Online

ACCESS | Metrics & More | Article Recommendations | Supporting Information

ABSTRACT: InGaZnO (IGZO)-based thin-film transistors and selector diodes are increasingly investigated for a broad range of applications such as high-resolution displays, high-density memories, and high-speed computing. However, its potential to be a key material for next-generation devices is strongly contingent on developing patterning processes with minimal damage at nanoscale dimensions. IGZO can be etched using CH_4-based plasma. Although the etched by-products are volatile, there remains a concern that passivation—an associated effect arising from the use of a hydrocarbon etchant—may inhibit the patterning process. However, there has been limited discussion on the CH_4-based etching of IGZO and the subsequent patterning challenges arising with pitch scaling (<200 nm). In this work, we systematically investigate dry chemical etching schemes to pattern an IGZO film into densely packed nanostructures using CH_4. Straight IGZO lines, ∼45 nm in width at a pitch of ∼135 nm, are produced by employing the traditional reactive ion etching method. While the passivating effect of CH_4 does not impede the etching process, any further shrinkage of feature and pitch dimensions amplifies reactive ion etching-induced damage in the form of profile distortion and residue redeposition. We show that this is efficiently addressed via atomic layer etching (ALE) of IGZO with CH_4 using a pulsed plasma. The unique combination of ALE and plasma pulsing enables controlled reduction of ion-assisted sputtering and redeposition of residues on the patterned IGZO features. This approach is highly scalable and is successfully applied here to achieve well-separated IGZO lines, with critical dimensions down to ∼20 nm at a dense pitch of ∼36 nm. These lines exhibit steep profiles (∼80°) and no undesirable change in IGZO composition post-patterning. Finally, ALE of IGZO under pulsed plasma, reproduced on 300 mm wafers, highlights its suitability in large-scale manufacturing for the intended applications.

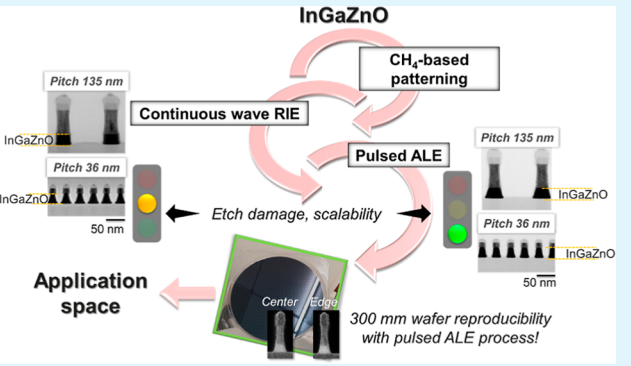

KEYWORDS: *atomic layer etching, pulsed plasma, IGZO, hydrocarbon etchant, scalability*

INTRODUCTION

InGaZnO (IGZO) has been garnering interest in recent years as a promising replacement for conventional amorphous silicon (aSi)-based semiconductor devices due to its inherent material properties. Increased carrier mobilities and current densities, better optical transmittance, and low OFF-state leakage currents makes this complex oxide system attractive for key applications ranging from thin-film transistors in high-definition transparent flat panel displays to high-speed Schottky diode selectors in high-density cross-point memories.[1−4] Its low-temperature processing makes its adoption into the back-end-of-line technology viable and being part of the next-generation chip integration a reality. This has recently boosted more research in its assimilation into advanced computing in memory designs for machine learning.[5] Although the application domain of IGZO keeps on expanding, one of the pivotal criteria for this material to realize its projected potential in manufacturable device concepts is its satisfactory patterning to smaller dimensions with minimal process-induced damage (PID).

The scaling of semiconductor technology nodes as well as the patterning roadmap of complex materials such as IGZO have predominantly been driven by the reactive ion etching (RIE) technique over the past decade. Commonly known halogen (F/Cl/Br)-based chemistries have been proposed to pattern IGZO via RIE.[6−9] To the best of our knowledge, the feature dimensions and pitches studied in these reports are above 200 nm.[9] Because these halogenated IGZO layers are non-volatile (Table 1),[10] significant amount of ion-assisted bombardment is required. Thus, ion-driven physical sputtering tends to overshadow the chemical component of RIE. Although the removal of the IGZO layer is facilitated, PIDs in the form of faceting, roughness, sidewall (SW) redeposition,

Received: April 28, 2022
Accepted: July 8, 2022

Table 1. Boiling Points (at Atmospheric Pressure) of IGZO-Based Etched By-Products Generated from the Reaction With F, Cl, Br, and CH_4[10]

	In		Ga		Zn	
	bonding	b.p. (°C)	bonding	b.p. (°C)	bonding	b.p. (°C)
F	InF_3	—	GaF_3	1000	ZnF_2	1500
Cl	$InCl_3$	800	$GaCl_3$	201	$ZnCl_2$	732
	$InBr_3$	—	$GaBr_3$	278	$ZnBr_2$	697
Br	InBr	656				
CH_4	$(CH_3)_3In$	136	$(CH_3)_3Ga$	56	$(CH_3)_3Zn$	46

and physical and chemical damage to the patterned IGZO layer come into prominence. Unfortunately, these issues are prone to intensify more as the critical dimensions (CDs) and pitches continue to undergo further shrinkage.

A few reports have suggested employing methane (CH_4)-based RIE for IGZO[11,12] instead of halogens. Hydrocarbon-based plasmas have previously been used for patterning the elements of IGZO independently, as part of optoelectronic materials such as InP, GaAs, and ZnO, among many other combinations.[13−15] The boiling points of the organometallic by-products formed from the reaction of In, Ga, and Zn with a hydrocarbon are comparatively lower in comparison to the halogenated counterparts (Table 1), thus the etching is anticipated to be more chemical than physical. However, as hydrocarbons are generally used as SW passivating agents during the patterning of dielectric, metal, and metal oxide features,[16] its etch inhibiting nature is presumed to come in conflict with its etching properties. So far, the literature reports on hydrocarbon-based patterning have been confined to low-density features with CDs in the order of few microns.[13−15] There is no documentation defining the feasibility and challenges of patterning IGZO with hydrocarbons as a function of CD and pitch. In this work, for the first time, we have carried out a systematic study on CH_4-based dry etching of IGZO targeting different pattern dimensions and densities employing conventional and advanced etch techniques as described below. It is revealed that IGZO can be patterned by using CH_4 without being adversely influenced by its inhibiting nature. Moreover, scaling down the feature CDs and pitches to few tens of nanometers is also achievable with this etchant.

The continuous wave (CW) RIE approach is initially studied to create IGZO lines/spaces. Although patterning of IGZO is attainable, undesirable effects such as ion-induced sputtering and redeposition of residues become easily noticeable at relaxed dimensions (CD ∼45 nm and pitch ∼135 nm). Undoubtedly, these effects increase and additional ones such as faceting and undercutting begin to occur as the dimensions are scaled down to <40 nm. In order to circumvent the PID from RIE both at relaxed and scaled dimensions, the patterning mechanism is substituted by a more advanced etching technique, that is, CW atomic layer etching (ALE).[17−23]

ALE promises a mechanism wherein etchant adsorption on the material surface, the subsequent reaction, and removal of the etched by-product can be deconvoluted and performed sequentially. It is self-limiting and has the potential to provide precise control of the etch depth down to angstrom level at low ion energies compared to RIE. While it has been extensively investigated since its first reporting three decades back, the etch gases studied for ALE of metal oxides or III−V compounds have mostly been halogen-based.[17,20−23] In addition, a significant proportion of these studies have focused on etching of either blanket films or relatively larger patterns at relaxed densities. Therefore, as ALE gains momentum as the preferred patterning method for compositionally complex materials in next-generation electronic applications, it becomes imperative to understand its potential and reproducibility at state-of-the-art pitches.

It is realized that the IGZO features patterned at 135 nm pitch by this gentle CW ALE method are still susceptible to significant residue redeposition. This provided a strong impetus to investigate ALE under a plasma[24,25] which is pulsed instead of being a continuous one. Under a pulsed plasma, additional flexibilities arising from the pulse frequency and duty cycle enable more meticulous tailoring of the etchant coverage across the material surface. More interestingly, it facilitates the modification of the ion flux composition dictating the removal mechanism of the etched by-products from the material surface. Hence, here the distinct advantages of ALE and pulsed plasma are harnessed together to demonstrate effective patterning of high-density IGZO lines using CH_4. Relatively straight (∼80°), well-isolated IGZO lines, which are as narrow as ∼20 nm, are achieved at a tight pitch of 36 nm. A significant minimization of pattern distortion and residue creation—pivotal to high performing devices at scaled densities—are realized with pulsed plasma-based ALE (pulsed ALE) of IGZO.

EXPERIMENTAL SECTION

Experimental Design. The hard mask (HM) strategies used for patterning IGZO lines/spaces are shown in Figure 1. Figure 1a depicts the trilayer HM stack used for patterning IGZO at a relaxed pitch of 135 nm. The line/space patterns are defined by a 193 nm immersion lithography tool. The HM is composed of SiO_2 (20 nm)/SiN (20 nm)/TiN (60 nm) (top to bottom) deposited atop a 30 nm thick IGZO layer. The IGZO film is amorphous and grown by physical vapor deposition at 300 °C. This HM strategy is chosen in order to be compatible with the integration schemes employed in semiconductor manufacturing. The SiN and SiO_2 layers usually act as sacrificial layers during planarization after the completion of both IGZO patterning and SiO_2 filling in the trenches between the lines. The exposed TiN surface can then be used for making electrical connections to the next metal layer in the chip.[4,26]

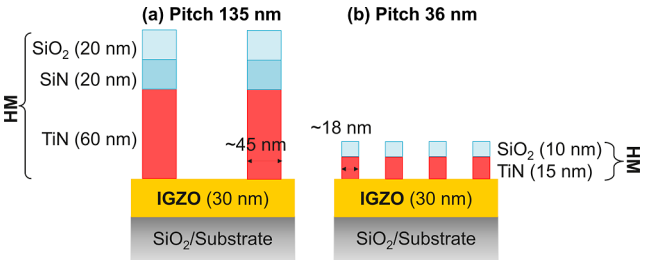

Figure 1. (a) HM stack used for IGZO patterning at a (a) pitch of 135 nm and at a (b) pitch of 36 nm.

Figure 1b shows the HM stack used for the study at a pitch of 36 nm. The line/space definition at this tight pitch is achieved through extreme ultraviolet lithography. In order to avoid any additional impact from the usage of high aspect ratio HM at tighter pitches, the HM design is simplified and composed of a thinner bilayer stack of SiO_2 (∼10 nm)/TiN (∼15 nm) (top to bottom). HM consumption is not anticipated as CH_4 is not capable of etching either SiO_2 or TiN. The IGZO film thickness remains constant throughout all experiments at different pitches.

https://doi.org/10.1021/acsami.2c07514
ACS Appl. Mater. Interfaces XXXX, XXX, XXX−XXX

Analytical Methods. For morphological investigations of the patterned HM stack and the IGZO features, scanning electron microscopy (SEM) is used. The cross-sectional SEM (X-SEM) images are obtained in backscattered electron mode to enhance the contrast between the different layers of the patterned feature. Transmission electron microscopy (TEM) is employed for higher resolution imaging of these IGZO patterns. TEM is equipped with energy-dispersive X-ray spectroscopy (EDS) for chemical analysis of the IGZO layer before and after patterning. It also enables the detection of any preferential elemental etching during the patterning process. The legends used in the figures depicting the EDS images and plots comprise the element and the corresponding X-ray spectral line studied here. The SEM and TEM tools used are VERIOS G4 and Titan G2 60−300, respectively, from ThermoFisher.

HM Patterning. Figure 2a shows the top view SEM image of the lines patterned at a pitch of 135 nm. The line/space CDs are

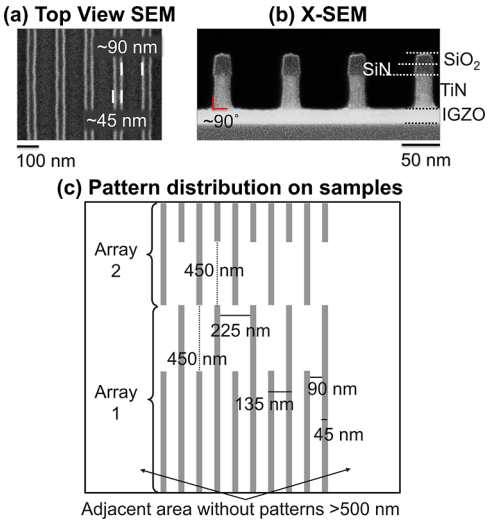

Figure 2. (a) Top view SEM and (b) X-SEM images of the patterned HM lines on IGZO at a pitch of 135 nm. (c) Pattern distribution and "area of interest" in this study.

estimated to be ∼45 and ∼90 nm, respectively, matching the initial lithography design values. Figure 2b displays the X-SEM image of the patterned HM. SiO_2 and SiN are patterned with a standard F-based chemistry.[27] A Cl/CH-based gas mixture is used for patterning the TiN layer.[28] The CH-based gas passivates the HM SWs during the etching process. The etching is well-controlled with no major recess observed in IGZO. The HM profile achieved is straight and provides a good reference point for the IGZO patterning study.

The arrangement of the HM patterns defined at 135 nm wide pitch on a sample is schematically presented in Figure 2c. The area of interest contains two consecutive arrays of parallel lines. The lines within the arrays are several micron long and arranged in a periodically staggered fashion. The adjacent regions on either side of the arrays are devoid of any HM patterns. This type of pattern distribution enables systematic examination of any pattern density-dependent etch rate, known as the loading effect,[29] arising from the etching process as the spacing between the features increases from 90 to 225 to >500 nm.

Figure 3 shows the top view and X-SEM images of the patterned HM at a pitch of 36 nm. The top view SEM (Figure 3a) image of the patterned HM on IGZO indicates that there is no bridging between these high-density lines. The bottom CD of the line is estimated to be ∼20 nm from the X-SEM image in Figure 3b, ∼3 nm larger than the top CD. Over-etching post-TiN layer patterning is carried out to guarantee that the HM lines at this tight pitch are well-separated. In the process, the IGZO layer is recessed by ∼8 nm. This is most likely from the use of CH_4, the SW passivating agent accompanying the Cl plasma to etch the TiN HM.

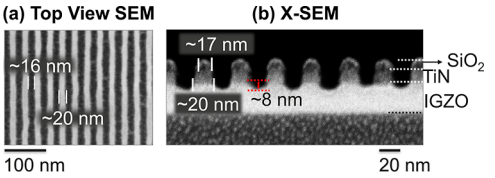

Figure 3. (a) Top view SEM and (b) X-SEM images of patterned HM lines on IGZO at a pitch of 36 nm.

Dry Etching of IGZO. Broadly, three different etching mechanisms are studied in this report−CW RIE, CW ALE, and pulsed ALE. A 13.56 MHz [radio frequency (RF)] inductively coupled plasma reactor from LAM Research dedicated for 300 mm diameter wafers is used in this study. The etch experiments are carried out on 2 x 2 cm^2 samples adhered to 300 mm Si carrier wafers. The etch gas chemistry used is CH_4/Ar. Ar has to be incorporated to maintain a stable plasma operation in the chamber throughout the etching duration. In addition, it is seen to be critical for diluting the hydrocarbon etchant and maintaining a reasonable etch rate particularly during RIE of IGZO.

Continuous Wave Reactive Ion Etching. The transformer coupled power (TCP) and the substrate bias are constant at 800 W and 120 V, respectively, during the RIE-based patterning study at 135 nm pitch. The other etch parameters including gas flow, pressure, temperature, and time are screened to target a reasonable etch performance (Table 2a). After the primary IGZO etch step, an O_2 plasma is applied to the sample for a short period to remove any excess of hydrocarbon passivation along the feature SWs to facilitate the morphological inspection of the patterned IGZO and of any sputtered residue formation. The patterning RIE process, eventually optimized for creating IGZO lines/spaces at a pitch of 135 and 36 nm, is cyclic in nature. The etching of the IGZO film is divided into shorter time intervals and alternated with an O_2 plasma. The process is schematically explained and tabulated in Table 2b.

Continuous Wave Atomic Layer Etching. This process comprises two steps. Step 1 involves reactant adsorption on the IGZO surface. Step 2 leads to etched by-product removal by a low-energy ion. Step 1and 2 are alternated until the IGZO film is patterned. The step sizes are generally in the order of few seconds. In our study, it is fixed at 5 s. The etching parameters used at a pitch of 135 nm are provided in Table 3.

Pulsed Atomic Layer Etching. The mechanism is similar to CW ALE, however, in this case, the plasma is subjected to pulsing. The pulsing frequency and duty cycle are set to 1 kHz and 30%, respectively. These conditions decide the ON time of the RF-based CW plasma. The optimal etching parameters generated in the study for pitch 135 and 36 nm are also provided in Table 3.

Similar to RIE, both ALE and pulsed ALE processes end with a final exposure to O_2 plasma. Though the optimized temperature tabulated is ∼120 °C, similar patterning performance can be achieved up to ∼140 °C. Unless specified, all X-SEM and TEM inspections are carried out after the samples have been exposed to O_2 plasma.

RESULTS AND DISCUSSION

Continuous Wave Reactive Ion Etching. For the first set of experiments, the CH_4 flow is screened to evaluate a threshold value at which chemical etching starts governing the IGZO patterning process. A suitable CH_4 flow is found within the range of ∼20−25 sccm and the CH_4/Ar ratio is maintained at ∼0.25. The gas pressure and temperature are fixed at 20 mT and 90 °C, respectively. The primary CH_4 dissociations anticipated in the plasma are as follows[30,31]

$$e^- + CH_4 \rightarrow CH_3^\bullet + H^\bullet + e^- \quad (1)$$

$$e^- + CH_4 \rightarrow CH_2^\bullet + H_2 + e^- \quad (2)$$

https://doi.org/10.1021/acsami.2c07514
ACS Appl. Mater. Interfaces XXXX, XXX, XXX−XXX

Table 2. (a) Etching Conditions for CW RIE. "*a*", "*b*"', "*c*", and "*t*" Represent the Variable Etching Parameters That Were Used for Studying Patterning of IGZO at a Pitch of 135 nm. An O_2 Plasma Was Applied Once the IGZO Film Was Fully Patterned Into Lines/Spaces. (b) Optimized Etch Conditions for Patterning IGZO Lines/Spaces at a Pitch of 135 and 36 nm Using Cyclic CW RIE[a]

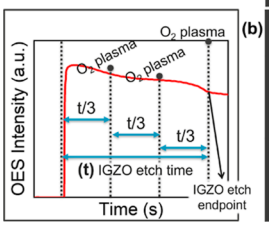

(a)

CW RIE	gas flow (sccm)	Pressure (mT)	TCP (W)	ESC bias (V)	Temp (°C)	Step time (s)
Pitch 135 nm	CH_4/Ar ('a')	'b'	800	120	'c'	't' (full etch)
	O_2 plasma applied after the IGZO features are completely patterned by the RIE process.					

(b)

Cyclic CW RIE	gas flow (sccm)	Pressure (mT)	TCP (W)	ESC bias (V)	Temp (°C)	Step time (s)	
Pitch 135 nm	CH_4/Ar (50/200)	40	800	120	≥120	40 (partial etch)	3 cycles
	O_2 (200)	10	800	0	≥120	30	
Pitch 36 nm	CH_4/Ar (40/200)	40	800	100	≥120	25 (partial etch)	4 cycles
	O_2 (200)	10	800	0	≥120	30	

[a]The schematic on the left represents the concept of cyclic etching used for IGZO here.

Table 3. Etching Conditions Used in Step 1 and 2 of ALE and Pulsed ALE of IGZO

Etch parameters		gas flow (sccm)	Pressure (mT)	TCP (W)	ESC bias (V)	Temp (°C)	Step time (s)
CW ALE Pitch 135 nm	Step 1	CH_4/Ar (20/200)	20	800	0	≥120	5
	Step 2	Ar (200)	10	800	65	≥120	5
Pulsed ALE Pitch 135 nm	Step 1	CH_4/Ar (20/200)	20	800	0	≥120	5
	Step 2	Ar (200)	10	700	100	≥120	5
Pulsed ALE Pitch 36 nm	Step 1	CH_4/Ar (15/150)	20	800	0	≥120	5
	Step 2	Ar (200)	10	700	100	≥120	5
O_2 plasma*		200	10	800	0	≥120	45

1kHz, 30% duty cycle

*used after the completion of both type of ALE process

$$e^- + CH_4 \rightarrow CH^\bullet + H_2 + H^\bullet + e^- \quad (3)$$

The $CH_3^\bullet$ radical is the most probable contributor in facilitating the volatile by-product creation listed in Table 1. The $CH_2^\bullet$ and $CH^\bullet$ species are expected to promote non-volatile by-product formation which can concurrently impede the etching process. The X-SEM image as shown in Figure 4a indicates that the 30 nm thick IGZO is patterned. However, the patterning is accompanied by a large taper of ∼50° and continuous residues along the entire surface area of the feature.

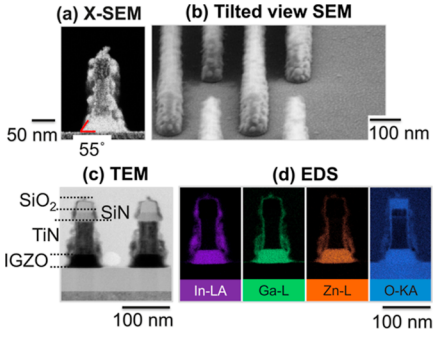

Figure 4. (a) X-SEM and (b) tilted view SEM results (after O_2 exposure) of patterned IGZO at a 135 nm pitch. A low CH_4 gas flow of ∼20 sccm, a low pressure of ∼20 mT, and a temperature of 90 °C are used in this experiment. (c) TEM and (d) EDS images of the IGZO patterned using the aforementioned conditions.

These residues are seen on multiple lines in the tilted view SEM image in Figure 4b. The tilted view SEM image also highlights the absence of differential etch rate between the line array and the adjacent area. To further understand the nature of these residues, TEM equipped with EDS is performed on this sample. The results are shown in Figure 4c,d. The elemental analysis from EDS reveals that the residues comprise elements of the IGZO layer. It may be elucidated that the relative concentration of $CH_3^\bullet$ to $CH_2^\bullet$ and $CH^\bullet$ reaching the IGZO surface is not sufficient to produce significant amount of volatile by-products. Furthermore, simultaneous ion-driven disintegration of these etched by-products and elements from the IGZO layer leads to residue redeposition along the feature's SW. These residues and deposition of hydrocarbon layer along the SW of the HM contribute to the tapered evolution of the IGZO line profile.

To test the premise, the pressure is doubled to ∼40 mT and the ESC temperature is increased to ≥120 °C to stimulate increased volatile by-product creation. X-SEM imaging carried out on these samples (Figure 5a) exhibited a substantial improvement in the IGZO line profile (85°). Residues are reduced and mostly concentrated on top of the SiO_2 HM. Also, the HM profile is well-preserved. The etch rate increases at the ∼90 nm wide spacings. Nevertheless, the tilted view SEM image in Figure 5a clearly shows that there is a severe macro-loading effect in the regions with larger open areas. As the spacing between the patterns increases beyond 90 nm, the IGZO film appears to undergo incomplete etching. The IGZO

https://doi.org/10.1021/acsami.2c07514
ACS Appl. Mater. Interfaces XXXX, XXX, XXX−XXX

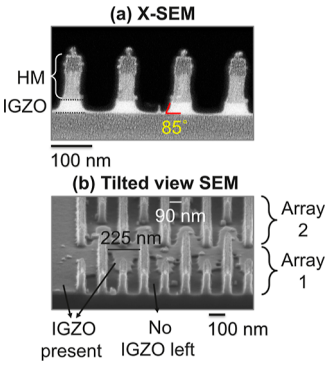

Figure 5. (a) X-SEM and (b) tilted view SEM results (after O_2 exposure) of patterned IGZO at a pitch of 135 nm. A low CH_4 gas flow of ~20 sccm, a high pressure of ~40 mT, and a temperature of 120 °C are used in this experiment.

layer still remains at the intersection between the two arrays of lines defined by ~225 nm wide spacing, as well as on the adjacent sides of the arrays. Although the relative increase in $CH_3^•$ compared to $CH_2^•$ and $CH^•$, brought about by the new set of etch parameters, efficiently removes IGZO from the ~90 nm wide spacings, the $CH_3^•$ concentration is not high enough to increase the etching performance in the larger open area at the same rate as the smaller spacings.

This macro-loading effect is alleviated by increasing the CH_4 gas flow by two-fold as evidenced in the tilted view SEM image presented in Figure 6a. The IGZO lines at a pitch of 135 nm

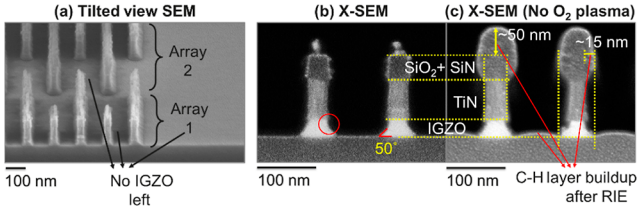

Figure 6. (a) Tilted view SEM image, (b) post-O_2 exposure X-SEM image, and (c) pre-O_2 exposure X-SEM image of patterned IGZO at a pitch of 135 nm. A high CH_4 gas flow of ~50 sccm, a high pressure of ~40 mT, and a temperature of 120 °C are used in this experiment.

still remain etched. However, the trade-off of using higher CH_4 flow lies in the appearance of the feature profile. As shown in Figure 6b, the patterned IGZO repossess back its taper of ~50°. Small amounts of residues are still visible along the exposed SiO_2 and SiN surface. In addition, there is a hint of an undercut (encircled in red) at the TiN/IGZO interface. To visualize better, the taper evolution of the IGZO line during the etching process, the experiment is repeated without the O_2 exposure step. A thicker Pt coating before X-SEM imaging (Figure 6c) enables clear observation of the residual hydrocarbon layer left on the sample post-patterning. As the etching process begins, concurrent to the residue redeposition on top of the HM, a portion of the isotropic hydrocarbon-based neutral flux generated deposits around the top of the HM. Hence, the trench opening between the features continuously shrinks for the ions and radicals incident toward the IGZO layer. In short, this lateral hydrocarbon growth across the SiO_2 and SiN surface contributes to the tapering of the patterned IGZO. Increased CH_4 flow also heightens the neutral flux scattering along the feature SWs in the trenches. In the process, the likelihood of lateral etching of IGZO can increase and therefore account for the slight undercut observed at the TiN/IGZO interface.

Cyclic Continuous Wave Reactive Ion Etching. In order to attack these residues above the HM as well as to rectify the IGZO profile, a cyclic RIE, schematically drawn and described in Table 2b, is performed. The IGZO is partially etched, and O_2 plasma is used for removing the surplus hydrocarbon deposit present around the HM as evidenced in Figure 6c. These two steps are repeated until the IGZO layer is completely removed.

Figure 7a shows the TEM result of the "cyclic RIE" process. Patterned IGZO lines with minimal tapering are obtained. The

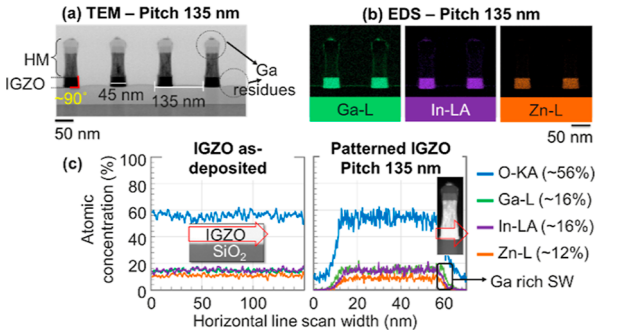

Figure 7. (a) TEM-based and (b) EDS-based chemical mapping of patterned IGZO at a pitch of 135 nm using "cyclic CW RIE". (c) EDS-aided horizontal elemental line scan across (left) an as-deposited (unpatterned) IGZO layer and (right) a patterned IGZO line of ~45 nm in CD.

three distinct layers of the HM are clearly seen. HM budget is well-preserved as the etchant used here is not expected to consume SiO_2 and SiN layers of the HM. However, the top of the HM appears faceted from more frequent exposure to ion bombardment due to the periodic removal of the hydrocarbon layer from top of the HM. EDS mapping as shown in Figure 7b reveals that the most dominant residues outlining the circumference of the HM stack and the spacing between the lines are Ga-based. Increased etching time is not useful as it promotes more sputtered residues. The bulk composition of IGZO before and after patterning is examined employing an EDS-based elemental line scan which is shown in Figure 7c. The composition of patterned IGZO matches closely that of the as-deposited film. The O signal measured across the patterned IGZO line is uniform indicating no significant depletion of oxygen from IGZO due to the occurrence of any hydrogen (from CH_4)-induced reduction of the semiconductor oxide. On the other hand, the SWs (~1−2 nm) of the patterned IGZO lines are Ga-rich. Therefore, although a vertical IGZO feature profile without any major loading effect is obtained, a critical shortcoming of this cyclic method is that the HM, IGZO SWs, and the regions between the lines are sputtered with a thin Ga layer. This can be attributed to a higher probability of ion-induced sputtering of Ga compared to In or Zn, thus creating a greater likelihood of its redeposition on any exposed surface (see Supporting Information, Figure S1). Therefore, the domination of ion bombardment-induced damage during RIE of IGZO is not completely suppressed and remains a challenge at this point in time.

Furthermore, it is observed that the process performance degrades with scaling (Figure 8). Figure 8a,b displays the performance of cyclic CW RIE at a pitch of 135 and 90 nm,

https://doi.org/10.1021/acsami.2c07514
ACS Appl. Mater. Interfaces XXXX, XXX, XXX−XXX

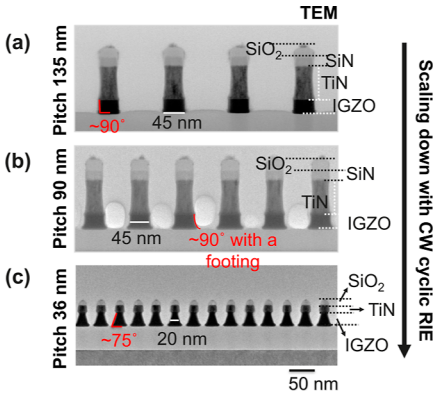

Figure 8. TEM images of IGZO lines/spaces patterned using cyclic CW RIE at a pitch of (a) 135, (b) 90, and (c) 36 nm.

respectively. Although the process conditions used at a pitch of 90 nm are identical to those used at a pitch of 135 nm (Table 2b), subtle differences are now seen in the profile of the 45 nm wide IGZO lines. A hint of an undercut in the IGZO profile at a pitch of 90 nm is seen along with a footing on the substrate (Figure 8b). The etching parameters are reevaluated for patterning the IGZO features at a drastically tighter a pitch of 36 nm (Table 2b). As seen in Figure 8c, the patterning performance does not improve. Instead, the undercut and footing observed at a pitch of 90 nm becomes more prominent at a pitch of 36 nm. The lines also become more tapered. These inadequacies in the patterning process emphasize the need to look beyond conventional RIE and investigate more advanced ALE-based processes. The next two sections will now focus on CH_4-based patterning of IGZO by ALE under CW and pulsed plasma modes.

Continuous Wave Atomic Layer Etching. One major issue highlighted above by RIE of IGZO at 135 nm pitch is sputtered Ga-rich residues along the SW of the patterned IGZO feature. As CW ALE provides the flexibility to achieve patterning at lower ion energies, it is envisioned that the creation of unwanted residues during the etching process can be significantly reduced. Figure 9a shows a schematic of CH_4-based CW ALE performed on an IGZO layer. Step 1 involves a continuous CH_4-based radical adsorption on the IGZO surface and step 2 comprises low-energy Ar ion bombardment of the by-product formed between the IGZO surface and the adsorbed CH_4-based radical. The ion energy is chosen to provide sufficient momentum to the etched by-product on the surface to be ejected without causing any undesired residue sputtering. This ensures a controlled layer-by-layer removal of the IGZO film. Because the goal is to deposit a thin hydrocarbon film closely mimicking a monolayer, the adsorption step 1 is driven at low pressure, low CH_4 flows, and without any substrate bias (Table 3). In order to confirm the synergy of the two steps in the CW ALE process, initially the adsorption step is exclusively repeated for 30 iterations on a 135 nm pitch structure (Figure 9b). The plasma conditions are deemed satisfactory as no spontaneous etching of IGZO is observed. The CH_4-based film deposits on all exposed surfaces of the HM and IGZO layer. It is noted that the deposition is not conformal. The deposited thickness is higher on top of the HM, than along its SWs or on top of the IGZO layer. The CH_4 deposition rate on IGZO is estimated to be ~0.11 nm/s. In the next stage, the ALE step 2 is exclusively repeated for 30 iterations (Figure 9c). The IGZO film still remains intact, however, the SiO_2 and SiN layer of the HM are sputtered and redeposited on the IGZO surface. The IGZO film is only removed when both ALE step 1 and 2 are repeated sequentially for a multiple number of times as shown in Figure 9d. An etch depth of ~0.75 nm is estimated after the completion of an ALE cycle (x) defined by one iteration each of ALE steps 1 and 2. The IGZO lines are fully patterned after 40 ALE cycles. The TEM image in Figure 9d shows that a reasonable line profile of ~80° is achieved for the IGZO features at a pitch of 135 nm. The tapering occurs due to the clogging effect from the passivation growth evolving along the HM SW (Figure 9b). The HM profile appears less faceted (TEM image, Figure 9d) compared to the profile achieved post-cyclic CW RIE (TEM image, Figure 7a). The IGZO film is effectively removed from both large and small spacings as is clearly seen from the tilted view SEM image in Figure 9b. However, particulate residues lining the SWs of the HM are clearly observed.

A detailed chemical analysis is then carried out on these patterned IGZO lines. The particulate residues on the HM SWs post-patterning are mapped using EDS in Figure 10a and

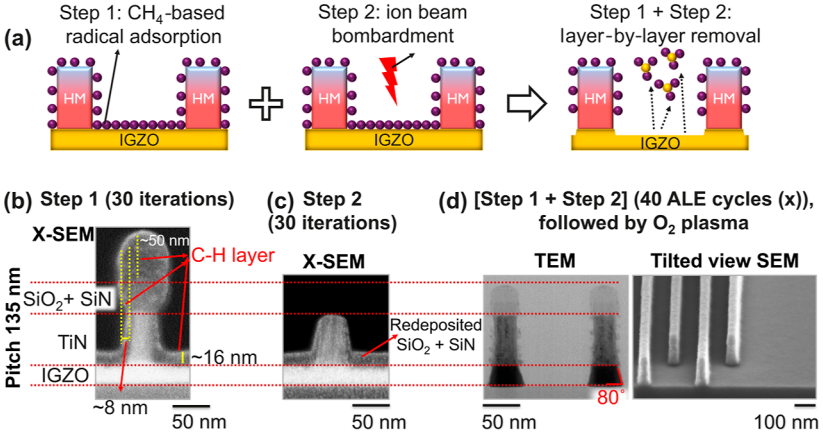

Figure 9. (a) Schematic representation of step 1 and 2 of ALE shown here for IGZO patterning using CH_4 as the etchant. (b) 30 iterations of "Step 1" of CW ALE only to understand the evolution of hydrocarbon growth on IGZO and the HM. (c) 30 iterations of "Step 2" of CW ALE only to understand the effect of Ar-induced sputtering on IGZO. (d) TEM and tilted view SEM images of patterned IGZO obtained after 40 CW ALE cycles.

https://doi.org/10.1021/acsami.2c07514
ACS Appl. Mater. Interfaces XXXX, XXX, XXX−XXX

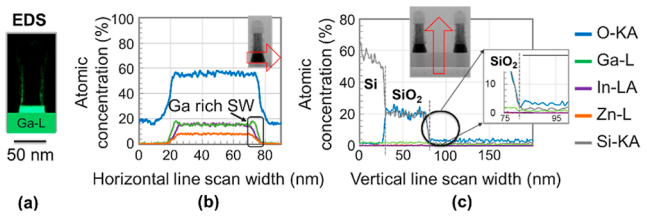

Figure 10. (a) EDS-based mapping of Ga residues on HM SW. (b) EDS-aided horizontal elemental line scan across a patterned IGZO line of CD ~45 nm. (c) EDS- aided vertical line scan of the region between IGZO lines, all acquired after patterning IGZO at a pitch of 135 nm using CW ALE.

are found to be largely Ga dominant (additional details in Supporting Information, Figure S2). The composition of the patterned IGZO structure is verified in Figure 10b. As is seen with RIE, the IGZO composition post-CW ALE remains intact whereas the IGZO SWs continue to be Ga rich. On the other hand, no residual peaks of redeposited In, Ga, or Zn are detected when an EDS-based vertical elemental line scan (Figure 10c) is performed in the spacing between two adjacent IGZO lines. Therefore, it can be summarized that though lower ion energies are useful in efficient etched by-product removal from the IGZO surface during ALE, Ga still remains sputtered along the SW of the HM. A potential cause can be that the ion energy used is still high to sputter out Ga while simultaneously aiding the volatile etched by-product removal from the modified IGZO surface. Nevertheless, compared to RIE, these residues are confined to lower number of exposed surfaces. It may be proposed to reduce the ion energy (substrate bias) further in ALE step 2 to mitigate the issues of Ga sputtering and redeposition, but this can severely impede the by-product removal. A more elegant approach is now to implement the ALE process under a pulsed plasma (pulsed ALE).

Pulsed Atomic Layer Etching. Plasma etching conditions can be modified effectually by tuning the frequency and duty cycle of the pulse applied over the TCP power and bias.[24] Independent control can be attained over ion-to-neutral ratios in the plasma, ion energies, and flux.[24,25] Figure 11 details the effect of plasma pulsing on steps 1 and 2 of an ALE process. In step 1, only the TCP power is pulsed as no bias is applied. The duty cycle of the pulse influences the dissociation of the gas molecules. Reduced (time-averaged) ON period compared to CW yields lower concentration of neutrals/radicals.[24,32] This is verified in the X-SEM image of the hydrocarbon deposited after 30 iterations of the pulsed ALE step 1 on the IGZO lines and spacings at a pitch of 135 nm (Figure 11a). The pulse frequency and duty cycle used in this work are 1 kHz and 30%, respectively. The hydrocarbon deposited atop the HM surface, along the HM SW, and on the IGZO surface is thinner compared to that attained post-step 1 of CW ALE in Figure 9b. Therefore, indirectly, the adsorbed etchant depth at the IGZO surface can be further controlled.[17,33] The $CH_3^•$ radical density is generally more abundant over $CH_2^•$ and $CH^•$ in RF discharges.[30,31] In addition, in the afterglow phase (RF OFF phase in a pulse period), the $CH_3^•$ radicals are expected to decay and are lost to the chamber walls at a slower rate, an order of magnitude lower than the other radicals, owing to lower surface loss and sticking coefficients.[31,34] Hence, even with thinner hydrocarbon adsorption occurring at every pulsed ALE step 1, $CH_3^•$ still remains the dominant species. This

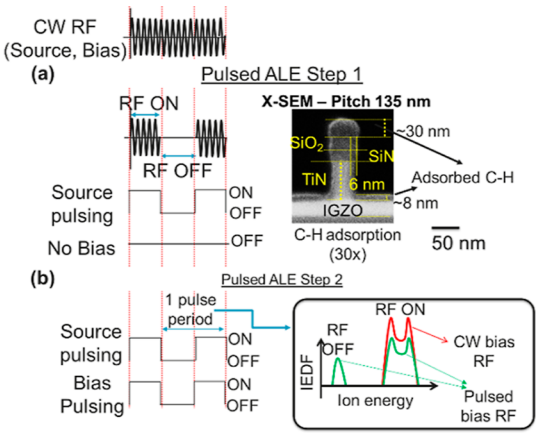

Figure 11. (a) Schematic representation of pulsing the CW RF source for application in Step 1 of pulsed ALE. The X-SEM image depicts the hydrocarbon adsorption over 30 iterations of Step 1 only in pulsed ALE at a pitch of 135 nm. (b) Schematic representation of pulsing the CW RF source and ESC bias (synchronous pulsing) for application in Step 2 of pulsed ALE. The variation in IEDF with ion energy as the plasma condition is changed from CW to pulsed mode is represented in the inset (outlined in black).

affirms more efficient generation of organometallic by-products from IGZO with plasma pulsing (Table 1). Moving to pulsed ALE step 2 employing Ar plasma (Figure 11b), both source and bias RFs are synchronously pulsed. The time-averaged ion energy distribution function (IEDF)[24] splits from bi- to trimodal. During the "RF ON" time, the positions of the high ion energy peaks will depend on the bias applied. The IEDF amplitude reduces with decreasing duty cycles. An energy dip to ~5−7 eV is estimated for the Ar ions left behind during the "RF OFF time" of the pulse.[24,35] Thus, in the case of Ar, even with the application of higher bias, the average IEDF over a single pulse period is lower for synchronously pulsed plasmas than for CW ones. The combination of high and low IEDF in a pulsed ALE step 2 provides a path to both efficiently remove the etched by-products from the IGZO surface and lower the probability of physically sputtering IGZO and HM. The disintegration of the volatile etched by-products leaving the IGZO surface is also lessened. Therefore, any sputter-induced faceting and redeposition along the exposed surfaces can be minimized with higher efficacy.

Figure 12 shows a "pulsed ALE" process flow which is used here for patterning IGZO lines at a pitch of 135 nm. The etch conditions are similar to CW ALE except for the adoption of higher RF bias in pulsed ALE step 2. The pulsed ALE steps are

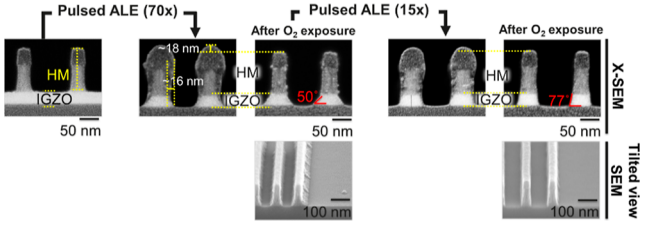

Figure 12. Process flow employed for CH_4-based pulsed ALE of IGZO at a pitch of 135 nm. The sequence comprises X-SEM image of the HM and X-SEM and tilted view SEM images of the IGZO lines and adjoining areas (before and after O_2 exposure) post 70 cycles, as well as post another additional 15 cycles of pulsed ALE.

https://doi.org/10.1021/acsami.2c07514
ACS Appl. Mater. Interfaces XXXX, XXX, XXX−XXX

sequentially repeated up to 70 iterations to pattern the 30 nm thick IGZO film. The etch rate is estimated to be ~0.4 nm/ALE cycle. X- SEM images before and after exposure to O_2 plasma enable to understand the evolution of the hydrocarbon buildup around the feature during the patterning process. The CH_4 adsorption on top of the HM appears more rounded and thinner after 70*x*, in contrast to the X-SEM observation after 30*x* in Figure 11a. This is because the thin adsorbed hydrocarbon layer is successively subjected to Ar ion impingement during each of the pulsed ALE cycles. However, the net lateral passivation growth around the HM over a period of 70 pulsed ALE cycles increases. This, in turn, is bound to influence the IGZO line profile at the bottom. The tapered profile of IGZO is measured to be ~50°. In the next stage, post exposure to O_2 plasma, 15 additional pulsed ALE cycles are repeated to rectify the IGZO taper to a more acceptable value of ~77°. This type of adjustment is not easily attainable with CW ALE. HM faceting and Si sputtering from the substrate underneath onto the SWs of IGZO occur due to the relatively higher bimodal IEDF at the same RF bias in CW plasma (Figure 11b). The tilted view SEM images confirm that the pulsed ALE conditions are optimal enough to prevent any loading effect in the large open areas adjacent to the array of lines.

Figure 13 provides a more exhaustive high-resolution morphological and chemical assessment on the performance

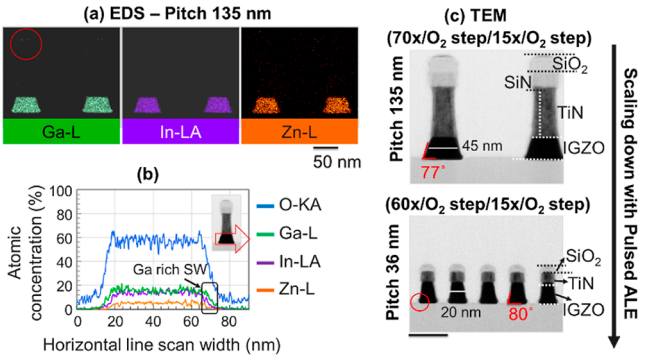

Figure 13. (a) EDS-based mapping of Ga, In, and Zn residues on HM SW and in the regions between the IGZO lines. (b) EDS-aided horizontal elemental line scan across a patterned IGZO line of CD ~45 nm, all acquired after patterning IGZO at a pitch of 135 nm using pulsed ALE. (c) TEM images of IGZO lines/spaces patterned at two different feature densities—pitch 135 and 36 nm—to investigate the scaling performance of pulsed ALE.

of pulsed ALE at a pitch of 135 nm. The elemental EDS mapping of the IGZO lines/spaces shown in Figure 13a detect no residues in the trenches between the lines. Compared to CW RIE and CW ALE, pulsed ALE led to the realization of almost residue-free HM surface and SWs. Only trace amounts of Ga, encircled in red in Figure 13a, are present on the HM (additional quantification in Supporting Information, Figure S3). The horizontal elemental line scan across the patterned IGZO as shown in Figure 13b confirms that the bulk IGZO composition is well-maintained. However, the issue concerning the IGZO lines exhibiting Ga-rich SWs is still not resolved. It seems that this effect may arise from a few more causes in addition to etching-induced Ga sputtering. The root cause is not known yet and is outside the scope of the current work. Nonetheless, it is clearly evident now that pulsed ALE is more robust in maintaining the integrity of the patterned features compared to the other counterparts discussed here. Figure 13c reinforces its reliability to be considered for high-density patterning down to a 36 nm pitch. Nearly all process parameters used to transfer the pulsed ALE process from pitch 135 to 36 nm are identical. The only difference is that the CH_4 flow used in the adsorption step 1 at a pitch of 36 nm is reduced. It is accompanied by a reduction in the Ar flow and therefore the CH_4/Ar ratio is equal to the one used for patterning at the larger pitch of 135 nm (see Table 3). The intermediate O_2 plasma step in pulsed ALE is also retained in order to target a good vertical profile for the IGZO lines at tight pitches. The total number of pulsed ALE cycles are decreased as the IGZO thickness to be etched now is ~23 nm instead of ~30 nm (Figure 3). Unlike RIE, degradation in the feature profile with scaling down of CD and pitch is not observed. Because both the aspect ratio of the HM and the etchant flow during the patterning process at a pitch of 36 nm are reduced, the hydrocarbon-induced clogging effect in the trenches between the lines is possibly less. Hence, the feature profile is not negatively impacted at such a dense pitch. A side effect of scaling observed here is a small yet visible micro-trenching at the foot of the IGZO line at a pitch of 36 nm (encircled in red, Figure 13c). This is earlier not visible at relaxed pitches. Nevertheless, it is now broadly established that pulsed ALE exhibits better and more scalable patterning properties compared to CW RIE. A detailed benchmarking of the process performances at a pitch of 36 nm is discussed below.

Direct Comparison of Cyclic CW RIE and Pulsed ALE at a Pitch of 36 nm. Figure 14a depicts the TEM images of the HM atop a blanket film of IGZO followed by TEM images of IGZO patterned by CW cyclic RIE and pulsed ALE. Small morphological differences on the appearance of the HM and IGZO profiles arising from the type of patterning technique used become clearly distinct.

- The SiO_2 HM becomes more rounded from ion bombardment and more prone to residue redeposition in CW cyclic RIE compared to pulsed ALE.
- The interface between the TiN and the IGZO layer displays a visible undercut in the case of CW cyclic RIE.
- A straighter IGZO profile with smaller footing is achieved with pulsed ALE.

The insets in Figure 14a containing the tilted view images of cyclic CW RIE and pulsed ALE show that the ordering of the lines is well-maintained, independent of the etching process used. The impact of cyclic CW RIE and pulsed ALE-based patterning on the bulk composition of IGZO, present in these ~20 nm sized lines, is verified from Figure 14b. The concentrations of In, Ga, Zn, and O after patterning with both these etching approaches closely match the values obtained for a blanket IGZO film. Unfortunately, the Ga-rich SWs (~2 nm) cannot yet be avoided.

The EDS-based vertical elemental mapping across the HM is carried out and shown in Figure 15 to investigate the residues observed on the HM post-IGZO patterning. Because the residue concentrations occurring on the HM are small-scale, the region of interest in the plots, encircled in black, are magnified and replotted. A background C signal is seen in these plots which is from the "spin-on-carbon" coating deposited on the samples during TEM sample preparation. The C signal is not subtracted in order to quantitatively compare the residues obtained from these two different

https://doi.org/10.1021/acsami.2c07514
ACS Appl. Mater. Interfaces XXXX, XXX, XXX−XXX

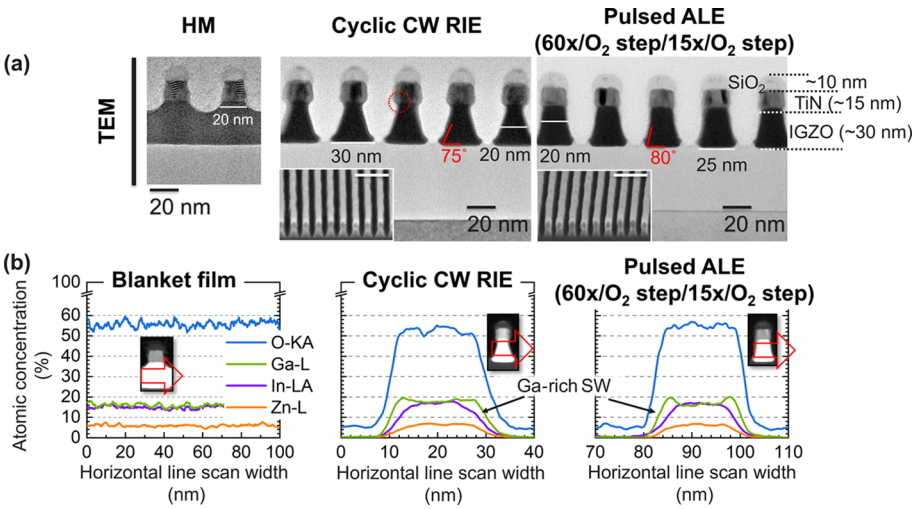

Figure 14. (a) TEM images of HM, IGZO patterned by cyclic CW RIE, and pulsed ALE at a pitch of 36 nm. Tilted view SEM images are shown in the insets (scale bar = 100 nm). (b) EDS-based horizontal elemental line scan across an unpatterned (blanket IGZO layer) and across a IGZO line of CD ~20 nm patterned using cyclic CW RIE and pulsed ALE at a pitch of 36 nm.

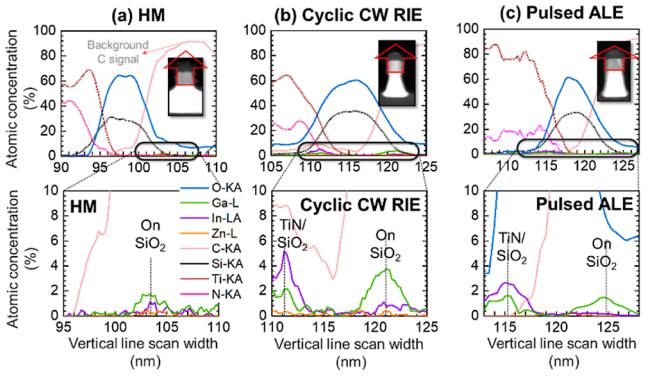

Figure 15. EDS-based vertical elemental line scan (across the HM) at a pitch of 36 nm: (a) after HM patterning; (b) after cyclic CW RIE of IGZO; and (c) after pulsed ALE (60x/O_2 step/15x/O_2 step) of IGZO. The regions encircled in black in each of the plots are magnified in the graphs below to show the residue mapping on top of the SiO_2 HM.

patterning approaches. The residue mapping across the HM before the patterning of IGZO (Figure 15a) is used as the reference in this study. Trace quantities of residues already exist on SiO_2 after HM patterning. These are <2% in atomic concentration and identified to be a mixture of In and Ga. This may have happened from a combination of unwanted physical and chemical etching of IGZO while patterning the TiN. When cyclic CW RIE is performed, the atomic concentration of Ga on the SiO_2 HM surface is more than double compared to pulsed ALE. An interesting observation is that residues are also noticed at the TiN/SiO_2 interface (Figure 15b). The nature of these residues at this interface is found to be In dominant. It may be hypothesized that at these small dimensions, the SiO_2 HM develops fissures from ion bombardment, thereby causing selective diffusion of some of the residues from an oxygen-rich surface to a nitrogen-rich one. This also emphasizes that at small pitches, the residues are no longer predominantly Ga-based. Sputtering and redeposition now comprise a mixture of In and Ga which are present in larger concentrations than Zn in the IGZO film. From Figure 15c, it is seen that residues on the HM, both on the SiO_2 surface and at the TiN/SiO_2 interface, are lesser with pulsed ALE. This reaffirms that the pulsed ALE approach causes less physical damage to the HM leading to lower chances of residue diffusion toward the TiN/SiO_2 interface.

A similar effective impact of the pulsed ALE approach is observed when scavenging for any residue traces in the spacings between the lines at these tight densities (Figure 16).

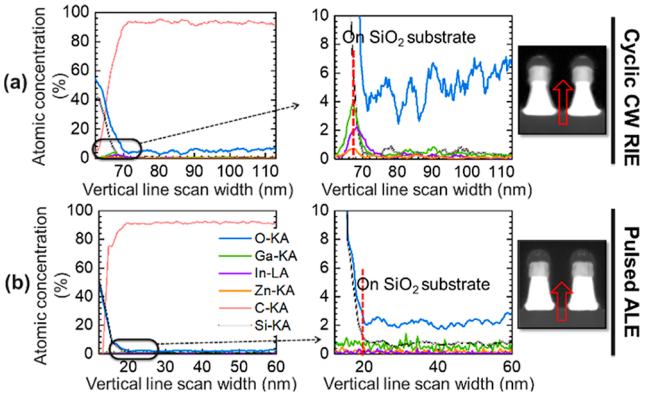

Figure 16. EDS-based elemental vertical scan is used for residue mapping in the region between two adjacent IGZO lines (~20 nm CD, pitch 36 nm): (a) after cyclic CW RIE and (b) after pulsed ALE (60x/O_2 step/15x/O_2 step). The encircled area in the plots shown on the left-hand side are magnified and shown in the plots on the right-hand side.

Similar to Figure 15, the background C signal is present in these plots. Zoomed-in images of the plots are also provided to observe the relative residue concentrations. The EDS elemental mapping detects residues deposited on the substrate between the lines for the cyclic CW RIE method (Figure 16a). The residues comprise In, Ga, and Zn with Ga present in larger quantity in line with the observations at larger pitches. On the contrary, well-separated IGZO lines are guaranteed with pulsed ALE as no elemental peaks from the semiconductor oxide are noted in the spacings between lines (Figure 16b).

Perspective on Throughput and Sustainability. With regard to throughput performance, it is estimated from Tables 2b and 3 that the patterning of IGZO at relaxed dimensions

https://doi.org/10.1021/acsami.2c07514
ACS Appl. Mater. Interfaces XXXX, XXX, XXX−XXX

(CD ∼45 nm) on smaller samples with the cyclic CW RIE approach is four times faster compared to pulsed ALE. In terms of assessing the environmental footprint of these etching techniques, that is, sustainable processing, the gas waste and emissions occurring during etching requires to be assessed. This is pivotal as the etchant CH_4 is a prominent greenhouse gas [global warming potential = 28 (for 100 years)].[36] An indirect assessment of these emissions is feasible by calculating from Tables 2b and 3, the total CH_4 gas volume (m^3) being used during etching. The volume of CH_4 used for patterning larger CDs (∼45 nm) on smaller samples, including the amount used during the stabilization of the gas flow, is ∼2 times higher for the pulsed ALE approach when compared to cyclic CW RIE.

However, these metrics change when transferring the processes to commercially used 300 mm wafers to assess large-scale reproducibility. The cyclic CW RIE process produces non-uniform patterning across the wafer, which is reduced by increasing both the gas flow (by ∼25%) and the number of cycles (∼6). The pulsed ALE process, owing to its intrinsic principles of operation, is transferred uniformly to a 300 mm wafer without the need of any additional changes. This reduces the throughput gap between the two patterning processes. In addition, the etchant volume consumed now during the cyclic CW RIE process surpasses the value used during pulsed ALE (by ∼1.2 times). Therefore, pulsed ALE of IGZO with CH_4 can be optimized further for a more favorable outlook toward cost-effectiveness and sustainability during large-scale wafer manufacturing in semiconductor technology.

CONCLUSIONS

In this work, a systematic assessment has been carried out for three different etching techniques employing CH_4 as the etchant. The three techniques, namely continuous wave RIE, continuous wave ALE, and ALE under a pulsed plasma, are used to pattern an IGZO layer into high-density nanostructures for pitch scaling below 200 nm. Contrary to expectation, any passivating effect induced by the hydrocarbon etchant does not create an etch blockade to adversely influence scaling of IGZO features at dense pitches. The RIE-based approach is found to be prone to high-energy ion-induced physical sputtering of IGZO and residue redeposition. These are alleviated by the use of the ALE technique under pulsed plasma. With this approach, well-separated IGZO lines are achieved down to a CD of ∼20 nm at a pitch of 36 nm. This high-density demonstration has been realized for the first time, to the best of our knowledge. It may also be feasible to fine-tune and extend this approach toward further shrinkage of IGZO features and feature densities.

In short, a reliable process window can be created with pulsed plasma-based ALE to uniformly pattern a wide range of feature CDs and densities, while continuing to nearly use the same set of etching parameters. This approach has the potential to be both manufacturing-friendly and sustainable. To conclude, these learnings can provide a window to explore the patterning of other IGZO-like complex alloy systems.

ASSOCIATED CONTENT

Supporting Information

The Supporting Information is available free of charge at https://pubs.acs.org/doi/10.1021/acsami.2c07514.

XPS depth profiling with Ar^+ ion to study enhanced sputtering of Ga from IGZO, additional EDS-based information for CW ALE and pulsed ALE, additional X-SEM images of ∼45 nm CD IGZO features patterned with pulsed ALE on 300 mm wafer, and ALE synergy quantification (PDF)

AUTHOR INFORMATION

Corresponding Author

Shreya Kundu − *IMEC, Leuven 3001, Belgium*; orcid.org/0000-0001-8052-7774; Email: Shreya.Kundu@imec.be

Authors

Stefan Decoster − *IMEC, Leuven 3001, Belgium*
Philippe Bezard − *IMEC, Leuven 3001, Belgium*
Ankit Nalin Mehta − *IMEC, Leuven 3001, Belgium*; orcid.org/0000-0002-2169-940X
Harold Dekkers − *IMEC, Leuven 3001, Belgium*
Frederic Lazzarino − *IMEC, Leuven 3001, Belgium*

Complete contact information is available at: https://pubs.acs.org/10.1021/acsami.2c07514

Author Contributions

All authors have given approval to the final version of the manuscript. All the images/artwork/photos that appear in the manuscript and Supporting Information file, including those in the TOC graphic, were created by the authors of this manuscript.

Notes

The authors declare no competing financial interest.

ACKNOWLEDGMENTS

The authors would like to thank Nouredine Rassoul (IMEC) for discussion on the HM strategy and Subhali Subhechha (IMEC) for providing a brief overview of the intended applications of IGZO. We acknowledge the support of IMEC's Industrial Affiliation Program and the Active Memory Program. We also acknowledge the support of IMEC's pilot line and SEM and MCA team for help with deposition and characterization processes.

REFERENCES

(1) Sheng, J.; Hong, T.-H.; Lee, H.-M.; Kim, K.-R.; Sasase, M.; Kim, J.; Hosono, H.; Park, J.-S. Amorphous IGZO TFT with High Mobility of ∼70 $cm^2/(V\ s)$ via Vertical Dimension Control Using PEALD. *ACS Appl. Mater. Interfaces* **2019**, *11*, 40300−40309.

(2) Dang, B.; Liu, K.; Zhu, J.; Xu, L.; Zhang, T.; Cheng, C.; Wang, H.; Yang, Y.; Hao, Y.; Huang, R. Stochastic Neuron Based on IGZO Schottky Diodes for Neuromorphic Computing. *APL Mater.* **2019**, *7*, 071114.

(3) Chand, U.; Fang, Z.; Chun-Kuei, C.; Luo, Y.; Veluri, H.; Sivan, M.; Feng, L. J.; Tsai, S.-H.; Wang, X.; Chakraborty, S.; Zamburg, E.; Thean, A. V.-Y. 2-Kbit Array of 3-D Monolithically-Stacked IGZO FETs with Low SS-64mV/dec, Ultra-Low-Leakage, Competitive μ-57 cm2/V-s Performance and Novel nMOS-Only Circuit Demonstration *2021 Symposium on VLSI Technology*; IEEE, 2021, pp 1−2.

(4) Belmonte, A.; Oh, H.; Rassoul, N.; Donadio, G. L.; Mitard, J.; Dekkers, H.; Delhougne, R.; Subhechha, S.; Chasin, A.; van Setten, M. J.; Kljucar, L.; Mao, M.; Puliyalil, H.; Pak, M.; Teugels, L.; Tsvetanova, D.; Banerjee, K.; Souriau, L.; Tokei, Z.; Goux, L.; Kar, G. S. Capacitor-Less, Long-RetentionDRAM Cell Paving the Way towards Low-Power and High-Density Monolithic 3D DRAM *2020 IEEE International Electron Devices Meeting (IEDM)*; IEEE, 400s2020, pp 28.2.1−28.2.4.

(5) Cosemans, S.; Verhoef, B.; Doevenspeck, J.; Papistas, I. A.; Catthoor, F.; Debacker, P.; Mallik, A.; Verkest, D. Towards 10000TOPS/W DNN Inference with Analog in-Memory Computing – A Circuit Blueprint, Device Options and Requirements *2019 IEEE International Electron Devices Meeting (IEDM)*; IEEE, 2019, pp 22.2.1–22.2.4.
(6) Joo, Y.-H.; Woo, J.-C.; Kim, C.-I. A Study of the Surface Chemical Reactions on IGZO Thin Film in BCl_3/Ar Inductively Coupled Plasma. *J. Electrochem. Soc.* **2012**, *159*, D190–D195.
(7) Park, J. C.; Jeong, O. G.; Kim, J. K.; Yun, Y.-H.; Pearton, S. P.; Cho, H. Comparison of Chlorine- and Fluorine-Based Inductively Coupled Plasmas for Dry Etching of InGaZnO4 Films. *Thin Solid Films* **2013**, *546*, 136–140.
(8) Park, W.; Whang, K. W.; Gwang Yoon, Y. G.; Hwan Kim, J. H.; Rha, S.-H.; Seong Hwang, C. S. High Rate Dry Etching of InGaZnO by BCl_3/O_2 Plasma. *Appl. Phys. Lett.* **2011**, *99*, 062110.
(9) Joo, Y.-H.; Woo, J.-C.; Kim, C.-I. Surface Reaction Effects on Dry Etching of IGZO Thin Films in N_2/BCl_3/Ar Plasma. *Microelectron. Eng.* **2013**, *112*, 74–79.
(10) Berger, L. I.; Covington, A. K.; Fox, R. B.; Frederikse, H. P. R.; Fuhr, J. R.; Goldberg, R. N.; Gschneidner, K. A.; Hammond, C. R.; Hampson, R. F.; Holden, N. E.; Donald Brooke Jenkins, H.; Kehiaian, H. V.; Alistair Kerr, J.; Kishore, N.; Lennen, R.; Lovas, F. J.; Martin, W. C.; Miller, J. S.; Miller, T. M.; Reader, J.; Snyder, L. E.; Stocker, D. W.; Taylor, B. N.; Trippe, T. G.; Vanýsek, P.; Wiese, W. L.; Wilks, E. S.; Wohlfarth, C.; *CRC Handbook of Chemistry and Physics*, 84th ed.; CRC Press, 2004, Section 3, 232–556, Section 4, 39–96.
(11) Zheng, Y.; Li, G.; Wang, W.; Li, X.; Jiang, Z. Dry Etching Characteristics of Amorphous Indium-Gallium-Zinc-Oxide Thin Films. *Plasma Sci. Technol.* **2012**, *14*, 915.
(12) Okuno, N.; Nei, K.; Honda, H.; Yamade, N.; Fujiki, H.; Semiconductor Device and Method for Manufacturing the Same. U.S. Patent 20,200,006,319 A1, February 2, 2021.
(13) Werking, J.; Schramm, J.; Nguyen, C.; Hu, E. L.; Kroemer, H. Methane/Hydrogen-Based Reactive Ion Etching of InAs, InP, GaAs, and GaSb. *Appl. Phys. Lett.* **1991**, *58*, 2003.
(14) Constantine, C.; Johnson, D.; Pearton, S. J.; Chakrabarti, U. K.; Emerson, A. B.; Hobson, W. S.; Kinsella, A. P. Plasma Etching of III-V Semiconductors in CH_4/H_2/Ar Electron Cyclotron Resonance Discharges. *J. Vac. Sci. Technol., B* **1990**, *8*, 596–606.
(15) Lee, J.-M.; Chang, K.-M.; Kim, K.-K.; Choi, W. K.; Park, S.-J. Dry Etching of ZnO Using an Inductively Coupled Plasma. *J. Electrochem. Soc.* **2001**, *148*, G1.
(16) Rolland, L.; Peignon, M. C.; Cardinaud, Ch.; Turban, C. SiO_2/Si Selectivity in High Density CHF_3/CH_4 Plasmas: Role of the Fluorocarbon Layer. *Microelectron. Eng.* **2000**, *53*, 375–379.
(17) Kanarik, K. J.; Lill, T.; Hudson, E. A.; Sriraman, S.; Tan, S.; Marks, J.; Vahedi, V.; Gottscho, R. A. Overview of Atomic Layer Etching in the Semiconductor Industry. *J. Vac. Sci. Technol., A* **2015**, *33*, 020802.
(18) Oehrlein, G. S.; Metzler, D.; Li, C. Atomic Layer Etching at the Tipping Point: An Overview. *ECS J. Solid State Sci. Technol.* **2015**, *4*, N5041–N5053.
(19) Carver, C. T.; Plombon, J. J.; Romero, P. E.; Suri, S.; Tronic, T. A.; Turkot, R. B., Jr. Atomic Layer Etching: An Industry Perspective. *ECS J. Solid State Sci. Technol.* **2015**, *4*, n5005–n5009.
(20) Metzler, D.; Bruce, R. L.; Engelmann, S.; Joseph, E. A.; Oehrlein, G. S. Fluorocarbon Assisted Atomic Layer Etching of SiO_2 Using Cyclic Ar/C_4F_8 Plasma. *J. Vac. Sci. Technol., A* **2014**, *32*, 020603.
(21) Metzler, D.; Li, C.; Engelmann, S.; Bruce, R. L.; Joseph, E. A.; Oehrlein, G. S. Fluorocarbon Assisted Atomic Layer Etching of SiO_2 and Si Using Cyclic Ar/C_4F_8 and Ar/CHF_3 plasma. *J. Vac. Sci. Technol., A* **2016**, *34*, 01B101.
(22) Park, S. D.; Oh, C. K.; Bae, J. W.; Yeom, G. Y.; Kim, T. W.; Song, J. I.; Jang, J. H. Atomic Layer Etching of InP Using a Low Angle Forward Reflected Ne Neutral Beam. *Appl. Phys. Lett.* **2006**, *89*, 043109.
(23) Park, S. D.; Lim, W. S.; Park, B. J.; Lee, H. C.; Bae, J. W.; Yeom, G. Y. Precise Depth Control and Low-Damage Atomic-Layer Etching of HfO[sub 2] using BCl[sub 3] and Ar Neutral Beam. *Electrochem. Solid-State Lett.* **2008**, *11*, H71–H73.
(24) Banna, S.; Agarwal, A.; Cunge, G.; Darnon, M.; Pargon, E.; Joubert, O. Pulsed High-Density Plasmas for Advanced Dry Etching Processes. *J. Vac. Sci. Technol., A* **2012**, *30*, 040801.
(25) Economou, D. J. Pulsed Plasma Etching for Semiconductor Manufacturing. *J. Phys. D: Appl. Phys.* **2014**, *47*, 303001.
(26) Zantye, P. B.; Kumar, A.; Sikder, A. K. Chemical Mechanical Planarization for Microelectronics Applications. *Mater. Sci. Eng.* **2004**, *45*, 89–220.
(27) Schaepkens, M.; Oehrlein, G. S. A Review of SiO_2 Etching Studies in Inductively Coupled Fluorocarbon Plasmas. *J. Electrochem. Soc.* **2001**, *148*, C211–C221.
(28) Tonotani, J.; Iwamoto, T.; Sato, F.; Hattori, K.; Ohmi, S.; Iwai, H. Dry Etching Characteristics of TiN Film Using Ar/CHF_3, Ar/Cl_2, and Ar/BCl_3 Gas Chemistries in an Inductively Coupled Plasma. *J. Vac. Sci. Technol., B* **2003**, *21*, 2163.
(29) Karttunen, J.; Kiihamaki, J.; Franssila, S. Loading Effects in Deep Silicon Etching. *Proc. SPIE, Micromachining and Microfabrication Process Technology VI* 2000, *4174*, 90–97
(30) Kojima, H.; Toyoda, H.; Sugai, H. Observation of CH_2 Radical and Comparison with CH_3 Radical in a RF Methane Discharge. *Appl. Phys. Lett.* **1989**, *55*, 1292–1294.
(31) Petrović, Z. Lj.; Bošković, B.; Jelenak, A.; Tomčik, B. Axial Distribution of Emission and Rate of Deposition of Diamond-Like Film in R.F. Discharges in CH_4. *Thin Solid Films* **1997**, *304*, 136–143.
(32) Bodart, P.; Brihoum, M.; Cunge, G.; Joubert, O.; Sadeghi, N. Analysis of Pulsed High-Density HBr and Cl_2 Plasmas: Impact of the Pulsing Parameters on the Radical Densities. *J. Appl. Phys.* **2011**, *110*, 113302.
(33) Brichon, P.; Despiau-Pujo, E.; Joubert, O. MD Simulations of Low Energy Cl_x^+ Ions Interaction with Ultrathin Silicon Layers for Advanced Etch Processes. *J. Vac. Sci. Technol., A* **2014**, *32*, 021301.
(34) Toyoda, H.; Kojima, H.; Sugai, H. Mass Spectroscopic Investigation of the CH_4 Radicals in a Methane RF Discharge. *Appl. Phys. Lett.* **1989**, *54*, 1507–1509.
(35) Brihoum, M.; Cunge, G.; Darnon, M.; Gahan, D.; Joubert, O.; Braithwaite, N. St. J. Ion Flux and Ion Distribution Function Measurements in Synchronously Pulsed Inductively Coupled Plasmas. *J. Vac. Sci. Technol., A* **2013**, *31*, 020604.
(36) Myhre, G.; Shindell, D.; Bréon, F.-M.; Collins, W.; Fuglestvedt, J.; Huang, J.; Koch, D.; Lamarque, J.-F.; Lee, D.; Mendoza, B.; Nakajima, T.; Robock, A.; Stephens, G.; Takemura, T.; Zhang, H. Chapter 8 Anthropogenic and Natural Radiative Forcing. *Climate Change 2013: The Physical Science Basis. Contribution Of Working Group I to the Fifth Assessment Report Of the Intergovernmental Panel On Climate Change*; Cambridge University Press: Cambridge, United Kingdom and New York, NY, USA, 2013, pp 659–740.

https://doi.org/10.1021/acsami.2c07514
ACS Appl. Mater. Interfaces XXXX, XXX, XXX–XXX